

Development of a Geant4 Simulation Platform of the HollandPTC R&D Proton Beamline for Radiobiological Studies

C.F. Groenendijk^a, M. Rovituso^b, D. Lathouwers^a, J.M.C. Brown^{c,a}

^a*Radiation Science & Technology, Delft University of Technology, Delft, The Netherlands*

^b*Research and Development, Holland Proton Therapy Centre, Delft, The Netherlands*

^c*Optical Sciences Centre, Department of Physics and Astronomy, School of Science, Swinburne University of Technology, Melbourne, Australia*

Abstract

Radiobiological studies represent an important step in obtaining a greater fundamental understanding of the differences between photon and proton radiotherapy on the cellular level. The Holland Proton Therapy Centre Delft (Netherlands) facilitates the performance of such radiobiological experiments through their dedicated R&D Beamline, but to take full advantage of this resource extensive characterisation of it is required. This work presents the development of a Geant4 simulation platform of the R&D Beamline to both characterise its performance, and enable the in-silico planning and optimisation of future radiobiological studies. The Geant4 platform was developed to simulate the R&D Beamline operating in both its pencil beam and passively scattered field configuration. Three different proton energy experimental datasets (70 MeV, 150 MeV and 240 MeV) of the pencil beam envelope evolution in free air and dose-depth profiles in water were used to train a six degree of freedom non-symmetrical Gaussian pencil beam surrogate model of the R&D Beamline proton source emitted from the Kapton vacuum pipe exit window. Benchmarking of the Geant4 platform was then undertaken with respect to three independent experimental datasets of the R&D Beamline operating in both its pencil beam at 120 and 200 MeV, and in its passively scattered field configuration at 150 MeV. A high level of agreement was found between the developed Geant4 platform and experimental data, with the following key physical parameters investigated: beam spot size and envelope evolution over depth, initial beam energy spread, depth dose distributions, and beam field uniformity. These results at intermediate energies proved that the developed simulation platform was capable of reproducing the beamline's characteristics, and therefore it will enable in-silico planning and optimisation of future radiobiological studies at HollandPTC.

Keywords: Proton Radiotherapy, Radiotherapy, Radiobiology, Geant4, HollandPTC

*Corresponding author: jmbrown@swin.edu.au

1. Introduction

Cancer patients treated with photon radiotherapy may experience severe radiation-induced side effects, drastically impacting quality of life [1]. In such cases, the physical characteristics of proton irradiation of tissue could play a significant role in the reduction of side effects by decreasing the average dose to healthy tissues surrounding the tumour, while applying the same or an increased dose to the tumour itself [2, 3]. However, even though proton radiotherapy is a promising treatment modality, it remains unclear whether this potential advantage of using protons over photons will lead to a significant improvement in patient outcome and quality of life (i.e. the reduction of severe side effects) [4, 5, 6]. To fully exploit the physical characteristics and enhance the effectiveness of proton radiotherapy, a greater understanding of the differences between photon and proton radiotherapy at the cellular level is required. At present a number of different clinical studies are ongoing to validate the benefit of protons regarding the reduction of severe side effects [7, 8, 9, 10, 11, 12, 13]. However, knowledge regarding DNA damage induction and involved repair pathways from proton and photon irradiation is lacking causing a challenge during patient treatment selection. The performance of fundamental radiobiological studies could contribute to reducing this knowledge gap and potentially improve the molecular level understanding of tumour response between these two radiation types.

The expansion of proton irradiation facilities across the globe represents a major step forward towards reaching this goal. Since 2018, the Holland Proton Therapy Centre Delft, Netherlands, (HollandPTC) has treated cancer patients that qualify for proton radiotherapy in the Netherlands [14]. HollandPTC was established not only to treat cancer patients, but also to carry out research to enhance the effectiveness of proton radiotherapy and investigate its cost-effectiveness and potential added value with respect to conventional photon radiotherapy. HollandPTC is a PROBEAM (Varian a Siemens Healthineers Company) isochronous cyclotron-based facility that features pencil beam scanning into two gantry rooms, one fixed horizontal eye treatment beamline, and one fixed horizontal Research & Development Beamline (R&D beamline) capable of producing proton energies ranging from 70 MeV up to 250 MeV. The R&D beamline, designed and developed specifically for HollandPTC, consists of equipment to build a passive scattering system in order to produce large fields of varying sizes to facilitate radiobiological studies. To carry out radiobiological experiments it is of great importance to have knowledge about the beamline's characteristics, performance and behaviour. For that reason, this work aims to characterise and develop an *in silico* Monte Carlo based simulation platform of the HollandPTC R&D beamline both to characterise and support the optimisation of future radiobiological experiments.

This work presents the development of a Geant4 [15, 16, 17] simulation platform of the HollandPTC R&D beamline. The development of this simulation platform is intended to both characterise the R&D beamlines performance, and

enable the in-silico planning and optimisation of future radiobiological studies at HollandPTC. Section 2 describes the development of the simulation platform, its training with respect to three proton energy experimental datasets, and then its benchmarking with respect to another three independent experimental datasets. The results of this simulation platform's training and benchmarking with respect to experimental measurements of the R&D beamline are then presented in Section 3. Finally, a combined discussion and conclusion then follows in Section 4.

2. Methods

The experimental room of the R&D beamline at HollandPTC is composed of a fixed horizontal proton nozzle that can deliver a therapeutic proton beam of energies between 70 and 250 MeV with beam currents at cyclotron extraction of 1 nA to 800 nA. At the exit window of the proton vacuum beam pipe a 3.8 meter long track of interchangeable modular tables with 750 mm \times 750 mm incorporated Thorlabs plates is present to support the construction of variety of different experimental apparatus. The present work focuses on the R&D beamline in its pencil beam and passively scattered field configuration. The passively scattered field configuration utilises the double scattering ring set up seen in Figure 1 to create a uniform field of varying size up to a limit of 200 mm \times 200 mm for radiobiological experiments. More details of about the R&D beamline at HollandPTC and its full range of capabilities can be found in Rovituso et al [18].

The methodology of this investigation towards the development and commissioning of the Geant4 simulation platform of the R&D beamline at HollandPTC can be divided into three phases: 1) simulation platform development, 2) training through comparison with three energy experimental datasets, and 3) benchmarking against three independent experimental datasets.

2.1. Phase 1: Geant4 Simulation Platform Development

Geant4 version 10.06.p01 [15, 16, 17] was utilised to develop the HollandPTC R&D beamline simulation platform based on the experimental geometry for the passively scattered field configuration seen in Figure 1. A total of 7 key geometric elements were implemented in the simulation platform that could be enabled/disabled depending on the beamline operational mode (i.e. pencil beam or passively scattered field configuration). These 7 elements shown in Figure 1 are: 1) the kapton vacuum pipe exit window, 2) 1st phase scattering foil, 3) beam monitor, 4) 2nd phase dual scattering ring, 5) initial stage beam defining brass collimator, 6) final stage beam defining brass collimator, and (7) the irradiation/measurement stage represented via a blue square box at its front surface. Here the 1st phase scattering foil and 2nd phase dual scattering ring facilitate the expansion and shaping of the initial proton pencil beam to generate a uniform intensity proton field. The scattered expanded beam is then collimated at two stages along its path through the use of a 1st stage static

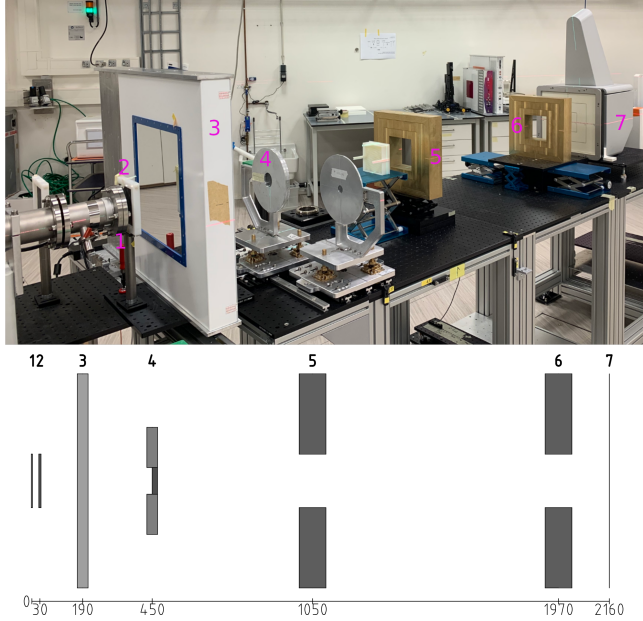


Figure 1: HollandPTC R&D beamline configured in its passively scattered field configuration (top). The 7 key geometric elements that were implemented in the Geant4 simulation platform to mimic this experimental configuration and their relative distances with respect to the kapton vacuum pipe exit window in mm (bottom). Here the 7 key geometric elements are: 1) the kapton vacuum pipe exit window, 2) 1st phase scattering foil, 3) beam monitor, 4) 2nd phase dual scattering ring, 5) initial stage beam defining collimator, and 6) final stage beam defining collimator, and 7) the front of the irradiation/measurement stage.

and 2nd stage variable open cross-section brass collimators to produce square uniform fields of up to 200 mm \times 200 mm. Table 1 outlines the dimensions and materials of first 6 different elements, with additional information relating to their design and orientation along the beamline's path outlined in Rovituso et al [18].

The non-symmetrical Gaussian pencil beam of HollandPTC R&D beamline was implemented using a six parameter surrogate model emerging at the kapton vacuum pipe exit window in three steps. In the first step the cross-sectional proton beam spot intensity was implemented via a two-dimensional Gaussian surrogate function of lateral width σ_x and lateral height σ_y . For the second step, the angular spread of the proton beam was modelled via a two-dimensional Gaussian surrogate function with angular spread in x and y of θ_x and θ_y respectively. Whereas in the third step, the characteristic energy spread of the cyclotron generated proton beam was modelled as a one-dimensional Gaussian distribution of initial mean energy E_0 and an energy spread ΔE . Finally, the transport of all particles was simulated using a combined Geant4 "Standard EM Option 4" and "QGSP_BIC_HP" physics list [17, 19] with atomic deexcitation enabled, a particle production range cut of 200 μm , and a low-energy cut off of

Element No.	Description	Dimensions	Material
1	Kapton Vacuum Pipe Exit Window	Disk (diameter,z): 100, 0.125 mm	G4_KAPTON
2	Scattering Foil	Box (x,y,z): 100, 100, 1.7 mm	G4_Pb
3	Beam Monitor	Surrogate Box (x,y,z): 400, 400, 0.6 mm	G4_WATER
4	Dual Scattering Ring	Inner Disk (diameter,z): 45, 5.5 mm Outer Ring (inn., out., z): 45, 200, 16 mm	G4_Pb G4_Al
5	1st Stage Collimator	Box Outer (x,y,z): 400, 400, 50 mm Inner Opening (x,y,z): 100, 100, 50 mm	Cu:Zn:Pb 58%:39%:3% Density: 8.7 g/cm ³
6	2nd Stage Collimator	Box Outer (x,y,z): 400, 400, 50 mm Inner Opening (x,y,z): 100, 100, 50 mm	Brass Cu:Zn:Pb 58%:39%:3% $\rho = 8.7 \text{ g/cm}^3$

Table 1: Number, description, dimensions, and materials of the geometric elements that were implemented in the Geant4 simulation platform to mimic the experimental configuration seen in Figure 1.

250 eV.

2.2. Phase 2: Simulation Platform Experimental Training

In the second phase of the simulation platform development, the six parameters of the non-symmetrical Gaussian pencil beam surrogate model were trained with respect to experimental measurements of the HollandPTC R&D beamline operating in a pencil beam configuration for initial mean proton beam energies of 70, 150 and 240 MeV. This was achieved through the training of σ_x , σ_y , θ_x and θ_y with respect to the beam envelope evolution in free air, and then the training of E_0 and ΔE with respect to the dose-depth profiles in water as illustrated in Figure 2.

Experimental measurement of the proton pencil beam envelope evolution in free air at 70, 150, and 240 MeV was undertaken using a Lynx® detector (IBA Dosimetry, Schwarzenbruck, Germany) placed at 230, 530, 911, 1230, 1530, 1830 and 2045 mm down-stream from the Kapton vacuum pipe exit window. In the Geant4 simulation platform the Lynx detector was implemented as a 300 mm \times 300 mm 1 mm thick PMMA protective layer in front of a 0.5 mm thick gadolinium-oxide layer scintillation screen with a 0.5 mm \times 0.5 mm pixelated image readout. Starting with (predefined) initial values for σ_x , σ_y , θ_x and θ_y from Rovituso et al [18], simulations of each mono-energetic pencil beam energy and Lynx detector offset distance were run using 10^6 protons. Both sets of experimental and simulated Lynx detector data 2D beam profiles were fitted with

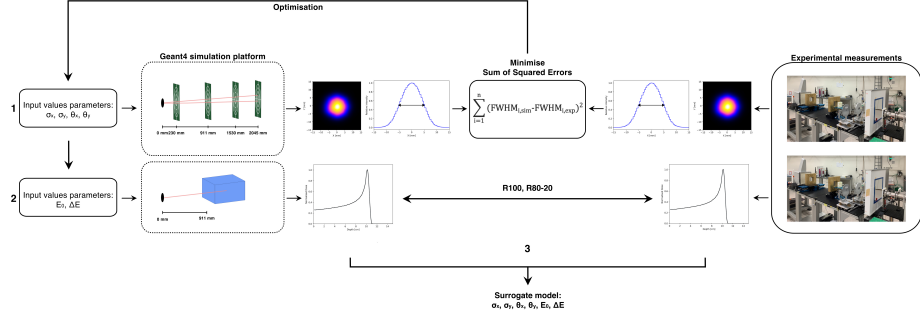


Figure 2: Scheme of the training phase. Starting at 1. Input parameters into the Geant4 simulation platform and the optimisation based on the SSE by a parameter sweep, 2. The sweep of varying initial energies and energy spread values, ending with 3. The creation of a surrogate model.

a 2D Gaussian function to obtain the Full Width at Half Maximum (FWHM) in x and y . The Full Width at Tenth Maximum (FWTM) was also extracted from the central x - and y -axis planes to investigate the tails of the distributions as a second merit. The agreement between experiment and simulation FWHM values as a function of the “semi mono-energetic” pencil beam energy was assessed through the use of the Sum of Squared Errors (SSE) metric:

$$\text{SSE} = \sum_{i=1}^n (\text{FWHM}_{i,\text{sim}} - \text{FWHM}_{i,\text{exp}})^2 \quad (1)$$

where $\text{FWHM}_{i,\text{sim}}$ is the simulated (“estimated”) FWHM and $\text{FWHM}_{i,\text{exp}}$ is the experimental (“true”) FWHM summed over n distances.

Optimisation of the σ_x , σ_y , θ_x and θ_y parameters for the Geant4 simulation platform was accomplished through a parameter sweep using the SSE metric in two steps. The first step consisted of a $\pm 10\%$ offset with respect to the initial values selected for the four parameters and resulted in a total of 81 combinations. The combination that resulted in the smallest SSE was taken as having the best agreement with experimental results and selected as the first estimate for the “true” parameter values. In the second stage, a second limited range parameter sweep of all four values was performed with a $\pm 5\%$ offset with respect to the first estimate of the “true” values to ensure that it was not a local minimum in the optimisation.

Experimental measurement of the proton pencil beam dose-depth profiles at 70, 150, and 240 MeV were obtained with a QubeNext (DE.TEC.TOR, Turin, Italy) placed at the beam isocentre 911 mm from the Kapton vacuum pipe exit window. The QubeNext detector possesses a $127 \text{ mm} \times 127 \text{ mm}$ sensitive area and has 128 layers of 2.34 mm thick detector planes/channels to yield proton water equivalent thickness of 310 mm. A $127 \text{ mm} \times 127 \text{ mm} \times 400 \text{ mm}$ water box was implemented in the Geant4 simulation platform 911 mm from the Kapton vacuum pipe exit window, and the central $6 \times 6 \text{ mm}$ cross-section region in step

1 mm along its depth was scored to emulate the QubeNext detector response. Starting with initial mean energy (E_0) and the energy spread (ΔE) estimates taken Rovituso et al [18] and optimised σ_x , σ_y , θ_x and θ_y parameters, 10^6 primary protons were simulated for each E_0 and ΔE combination which were varied in steps of 0.1 MeV around these initial estimates. The experimental and simulated proton pencil beam dose-depth profile data was fitted with a Bortfeld function [20], and the R80 proton range, R80-R20 distal fall-off, and peak-to-entrance ratio extracted as figures of merit to optimise E_0 , ΔE , and to provide a general figure of merit for both these two parameters in combination. Here R80 represented the depth along the beam central axis in water to the distal 80 percent point of the maximum dose, and R80-R20 the variation in the Bragg peak's distal fall of width.

The final step of Geant4 simulation platform training phase was to developed energy dependent surrogate functions for each the six parameter inputs for the non-symmetrical Gaussian pencil beam of HollandPTC R&D beamline. These surrogate functions were developed through fitting second-order polynomial functions to the obtained optimised beam parameters values at 70, 150 and 240 MeV. With these functions the Geant4 simulation platform only requires the HollandPTC's cyclotron mean extraction proton energy to model emerging proton beam structure, energy, and energy spread at the Kapton vacuum pipe exit window of the R&D beamline.

2.3. Phase 3: Simulation Platform Experimental Benchmarking

The third, and final, phase in the development and commissioning of the Geant4 simulation platform was to experimental benchmark performance with respect to three independent experimental datasets. Two of these datasets were of the HollandPTC R&D beamline operating in its pencil beam configuration at 120 and 150 MeV, and the other was the HollandPTC R&D beamline operating in its passively scattered field configuration at to generated a $100\text{ mm} \times 100\text{ mm}$ field at the irradiation/measurement stage for a cyclotron mean extraction proton energy of 150 MeV.

Experimental measurements and simulation with the completed Geant4 simulation platform were undertaken at 120 and 150 MeV in an identical manner to that outlined above to obtain the beam envelope evolution in free air and dose-depth profiles in water datasets. With the completed Geant4 simulation platform, a total of 5×10^6 protons were run for each energy and Lynx detector offset position combination, and 10^6 protons at each energy for the dose-depth profile data. The experimental and simulated FWHM, FWTM, depth at maximum dose, and distal fall off at each energy were compared to assess the validity of the developed HollandPTC R&D beamline Geant4 simulation platform operating in pencil beam configuration.

The experimental measurement of the $100\text{ mm} \times 100\text{ mm}$ field generated at the irradiation/measurement stage for the HollandPTC R&D beamline operating in its passively scattered field configuration was undertaken using the Lynx detector at 150 MeV. Large field simulations were also performed at 150 MeV with all beam elements implemented as shown in Figure 1 and for an inner

open cross-section of the final stage beam defining brass collimator set to 100 mm \times 100 mm. A uniformity (U) figure of merit across the field for both the experimental and simulation data was calculated by:

$$U [\%] = \left(1 - \frac{I_{max} - I_{min}}{I_{max} + I_{min}} \right) \cdot 100\% \quad (2)$$

where I_{max} is the maximum intensity across the field, and I_{min} is the minimum intensity across the field. It should be noted that a uniformity of above 97% is required for radiobiological experiments. The experimental and simulated uniformity values, and x and y axis central beam profiles were compared to assess the validity of the developed HollandPTC R&D beamline Geant4 simulation platform operating in a passively scattered field configuration.

3. Results

3.1. Simulation Platform Experimental Training

The values for the non-symmetrical Gaussian pencil beam surrogate model parameters σ_x , σ_y , θ_x and θ_y obtained through the two-fold parameter sweep at 70, 150 and 240 MeV can be seen in Table 2. All four of these beam parameter show a decreasing trend with increasing initial mean proton energy.

E (MeV)	σ_x (mm)	σ_y (mm)	θ_x (rad)	θ_y (rad)	E_0 (MeV)	ΔE (MeV)
70	3.383	2.559	0.00371	0.00409	69.8	1.43
150	2.819	2.100	0.00280	0.00330	148.8	1.35
240	2.509	1.890	0.00273	0.00300	235.5	0.8

Table 2: Optimised non-symmetrical Gaussian pencil beam surrogate model parameters at 70, 150 and 240 MeV: lateral spread σ in x and y (mm) and angular spread θ in x and y (radians), initial mean energy E_0 (MeV) and energy spread ΔE (MeV).

Figure 3 presents the experimental and Geant4 2D beam cross-sections and their x -axis line profiles measured closest to the Kapton exit window (230 mm), at the isocentre (911 mm) and furthest from the exit window (2045 mm) for the 70 MeV, 150 MeV and 240 MeV datasets. Here the 2D beam cross-sections are visualised with contour lines to help assess the shape of the intensity profile more easily, with a line profile through the centre (x -axis) of the experimental and Geant4 profiles visualised in the third row of each sub-figure. Inspection of these results illustrate that the shape of the Geant4 2D beam cross-sectional intensity profiles possess a high level of correlation with respect to the structure of the experimental profiles. Due to the configuration of the beam defining optics, the 2D beam cross-section for each energy consists of a larger lateral width (x) closest to the Kapton exit window, an almost symmetric beam profile at the isocentre, and a larger lateral height (y) downstream of the beamline. For example, in the 150 MeV 2D beam cross-section $FWHM_x$ increases from 6.8 mm to 9.5 mm to 17.6 mm, and the $FWHM_y$ increases from 5.3 mm to 9.3 mm to 18.9 mm, at 230, 911 and 2045 mm respectively.

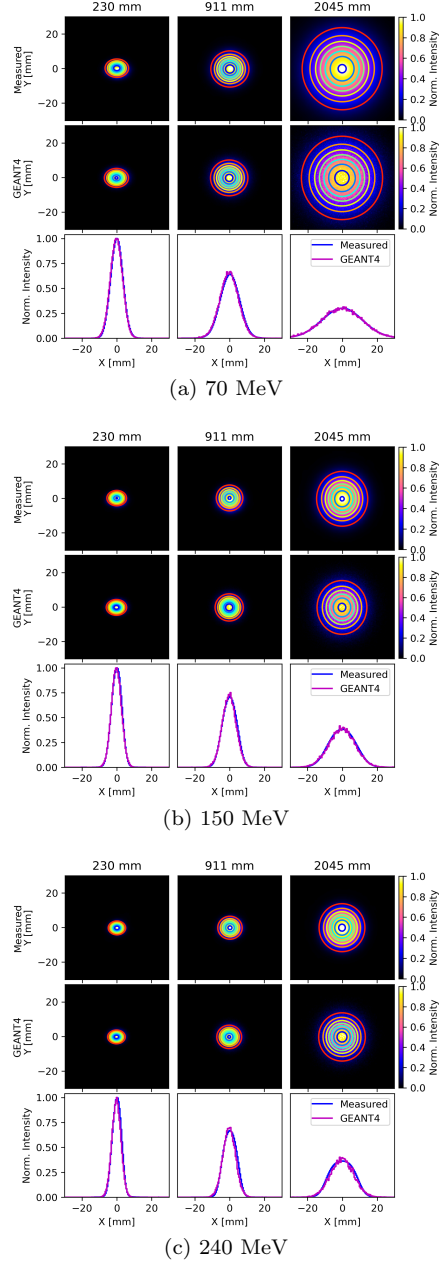


Figure 3: The experimental and Geant4 two dimensional proton beam intensity cross-sections and line profiles through the centre (x -axis) at 230, 911 and 2045 mm for the (a) 70 MeV, (b) 150 MeV and (c) 240 MeV.

E [MeV]	R80 [cm]		R80-R20 [cm]		Peak-Entrance ratio	
	Exp.	Geant4	Exp.	Geant4	Exp.	Geant4
70	3.91	3.96	0.16	0.21	3.4	3.6
150	15.52	15.52	0.38	0.38	3.4	3.4
240	34.36	34.38	0.54	0.50	3.2	3.4

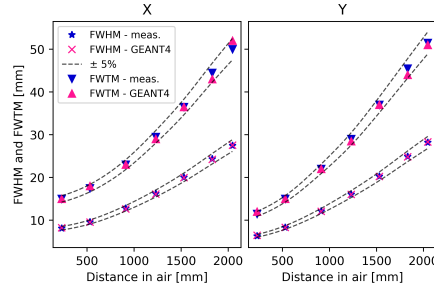
Table 3: Proton range R80 [cm], distal fall-off R80-R20 [cm] and peak-to-entrance ratios of the experimental and Geant4 of the 70, 150, and 240 MeV depth-dose distributions seen in Figure 5.

The 2D Gaussian fitted FWHM and the FWTM values extracted from the central x and y line profiles for the 70, 150, and 240 MeV datasets can be seen in Figure 4. The dotted lines represent a $\pm 5\%$ deviation with respect to experimental results to aid in assessing the accuracy of the Geant4 results. For all energies the Geant4 FWHM values in both x and y were reproduced to within less than 5% (approximately $\pm 2\%$). Analysis of the FWHM at isocentre with energy illustrates that the FWHM_x in experimental results decreases from 12.8 mm to 9.5 mm to 8.6 mm, whereas the Geant4 results decreases from 12.6 mm to 9.4 mm to 8.5 mm for the 70, 150 and 240 MeV datasets respectively. A similar trend can be seen in FWHM_y isocentre data with the experimental and Geant4 results decreasing from 12.2 mm to 9.3 mm to 8.1 mm, and 12.1 mm to 9.1 mm to 8.0 mm for the 70, 150 and 240 MeV datasets respectively. However, there is a reduced level of correlation between experimental and Geant4 FWTM values. At 70 and 150 MeV the difference was still within 5% of measured results, but at 240 MeV the difference was within 9% with the tails of the Geant4 distributions generally being wider than the experimental distributions.

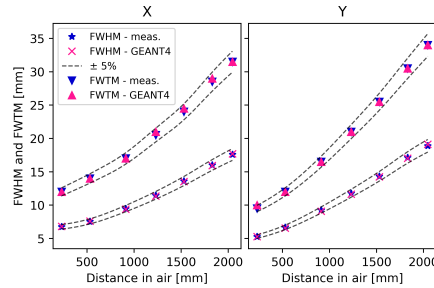
Table 2 summarises the initial mean energies (E_0) and accompanying energy spreads (ΔE) after tuning the proton range (R80) and distal fall-off. The depth-dose distributions of experimental and Geant4 results obtained with these optimised values are shown in Figure 5, and their corresponding proton range (R80), distal fall-off (R80-R20) and peak-to-entrance ratio values is displayed in Table 3. The depth-dose profiles are normalised on the maximum dose and show agreement in R80 to within 0.5 mm for all energies. The distal fall-off at 70 MeV agrees within 0.5 mm, at 150 MeV the distal fall-offs are equal, and at 240 MeV the offset is within 0.5 mm. At higher energies, an increase in peak width is observed due to range straggling. The small discrepancies in the simulation and Geant4 data that exist in the range and distal fall-off can be attributed to uncertainties in the alignment and the resolution of the QUBEnext detector. Overall a high level of correlation can be seen between the experimental and Geant4 depth-dose profiles at 70, 150, and 240 MeV.

3.2. Simulation Platform Experimental Benchmarking

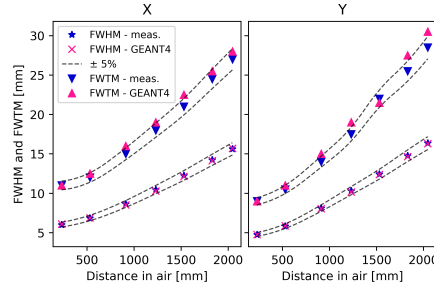
Table 4 presents the utilised 120 and 200 MeV non-symmetrical Gaussian pencil beam parameters in the Geant4 simulations that were obtained with the



(a) 70 MeV



(b) 150 MeV



(c) 240 MeV

Figure 4: Experimental and Geant4 2D beam cross-section FWHM and FWTM values as a function of distance from the Kapton vacuum pipe exit window at 70, 150 and 240 MeV. Here error bars representing the accuracy of FWHM data fitting cannot be resolved due to their scale being on the same order as FWHM data symbols.

developed energy dependent surrogate functions (see Section 2.2). The experimental and Geant4 beam envelope evolution at seven distances from the Kapton exit window were studied for each energy, with their 2D beam intensity cross-sections and central line profiles at 230, 911 and 2045 mm presented in Figure 6. A high level of correlation can be observed in the 120 and 200 MeV experimental and Geant4 data shown in Figure 6 at all three distances. Additionally, a higher level of beam divergence in y than x as a function of distance from the

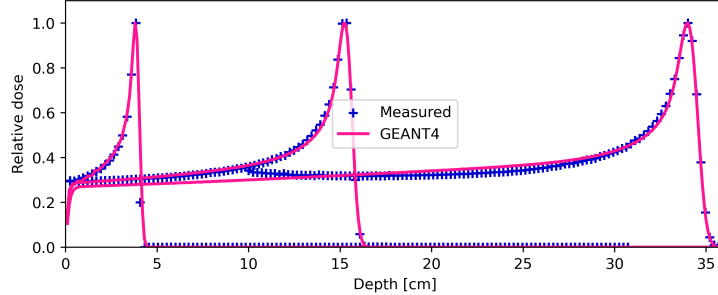


Figure 5: Experimental and Geant4 depth-dose profiles in “water” at 70, 150, 240 MeV.

Kapton exit window can be seen corresponding to the observed beam envelope evolution behaviour in Figure 3.

E (MeV)	σ_x (mm)	σ_y (mm)	θ_x (rad)	θ_y (rad)	E_0 (MeV)	ΔE (MeV)
120	2.998	2.242	0.00304	0.00353	119.4	.43
200	2.604	1.943	0.00264	0.00306	197.3	1.1

Table 4: Geant4 non-symmetrical Gaussian pencil beam parameters utilised at 120 and 200 MeV : lateral spread σ in x and y (mm) and angular spread θ in x and y (radians), initial mean energy E_0 (MeV) and energy spread ΔE (MeV).

The 2D Gaussian fitted FWHM and the FWTM values extracted from the central x - and y -axis line profiles for the 120, and 200 MeV datasets can be seen in Figure 7. Again, here the dotted lines represent a $\pm 5\%$ deviation with respect to experimental results to aid in assessing the accuracy of the Geant4 results. Inspection of Figure 7 shows that the Geant4 FWHM values in both x and y were reproduced to within 5% of the experimental data at the 120 and 200 MeV. However, there is a reduced level of correlation between experimental and Geant4 FWTM values that is dominated via the 7.6% difference in the y FWTM at distance 1830 mm in the 120 MeV data. Overall there is a high level of correlation between the experimental and Geant4 datasets at both 120 and 200 MeV. This proves that the developed Geant4 simulation platform is able to reproduce the beam envelope evolution behaviour for initial mean beam energies between 70 and 240 MeV of the R&D beamline at HollandPTC operating in its pencil beam configuration.

The experimental and Geant4 depth-dose profiles at 120 and 200 MeV can be seen in Figure 8. In the 120 MeV depth-dose profiles the Geant4 proton range agrees to within 0.5 mm of the experimental proton range, and their distal fall-off does not deviate from one another. Whereas for the 200 MeV depth-dose profiles, the Geant4 proton range is within 1.5 mm to the experimental value and it’s distal fall-off less than 1 mm smaller than the experimental value. Again, these differences in experimental and Geant4 dose-depth profiles can be primarily attributed to uncertainties in the alignment and the resolution of the

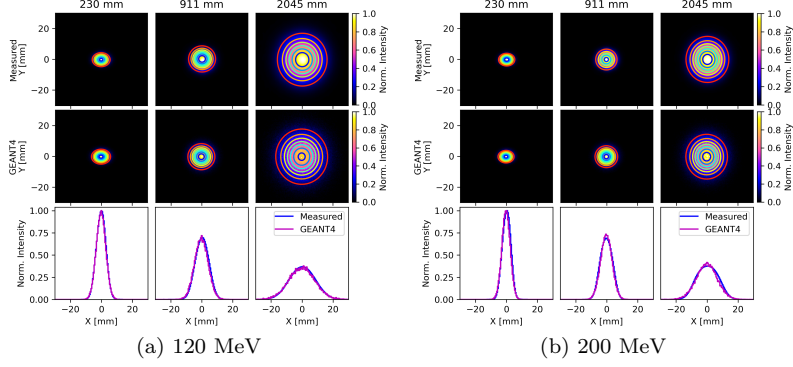


Figure 6: The experimental and Geant4 two dimensional proton beam intensity cross-sections and line profiles through the centre (x -axis) at 230, 911 and 2045 mm for the (a) 120 MeV, and (b) 200 MeV.

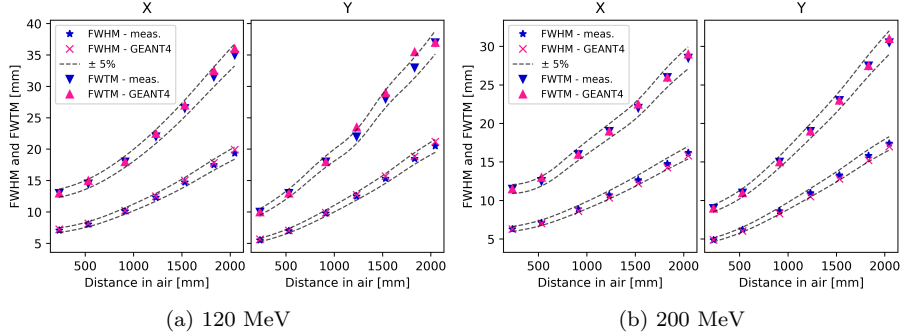


Figure 7: Experimental and Geant4 2D beam cross-section FWHM and FWTM values as a function of distance from the Kapton vacuum pipe exit window at 120, and 200 MeV. Here error bars representing the accuracy of FWHM data fitting cannot be resolved due to their scale being on the same order as FWHM data symbols.

QUBEnext detector. The proton range (R80), distal fall-off (R80-R20) and peak-to-entrance ratio at these energies for both the experimental and Geant4 depth-dose profiles can be found in Table 5. Overall there is a high level of correlation that can be seen between the experimental and Geant4 depth-dose profiles at both 120 and 200 MeV, further proving that the developed Geant4 simulation platform is able to accurately model the R&D beamline at HollandPTC operating in its pencil beam configuration.

Finally, the experimental and Geant4 100 mm \times 100 mm fields and their respective central x -axis lines profiles generated at the irradiation/measurement stage of the HollandPTC R&D beamline operating in its passively scattered field configuration can be seen in Figure 9. Qualitative comparison of the experimental and Geant4 2D intensity maps shows a high level of correlation in the

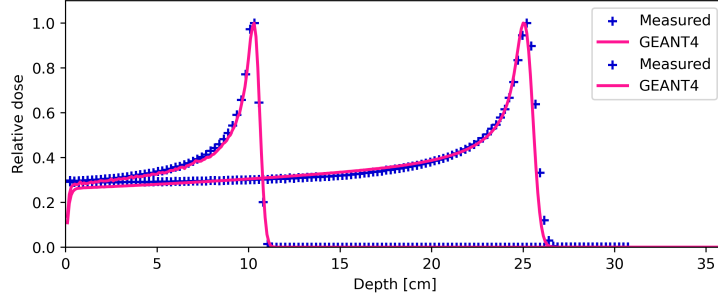


Figure 8: Experimental and Geant4 depth-dose profiles in “water” at 120 and 200 MeV.

E [MeV]	R80 [cm]		R80-R20 [cm]		Peak-Entrance ratio	
	Meas.	Geant4	Meas.	Geant4	Meas.	Geant4
120	10.47	10.50	0.33	0.33	3.4	3.6
200	25.54	25.39	0.51	0.45	3.5	3.6

Table 5: Proton range R80 [cm], distal fall-off R80-R20 [cm] and peak-to-entrance ratios of the experimental and Geant4 of the 120 and 200 MeV depth-dose distributions seen in Figure 8.

field shape and intensity. In addition, their central x -axis lines profiles shown in the bottom row of Figure 9 show a high level of correlation with slight deviation at the field edges. Assessment of the field uniformity for the experimental data yields a x - and y -axis value of 97.4% and 97.7% respectively. Whereas the field uniformity of the Geant4 data is 96.7% and 96.9% in x - and y -axis respectively. This less than 1% field uniformity different in along both axis, and high level of qualitative correlation in the 2D intensity maps and x -axis lines profiles proves that the developed Geant4 simulation platform is able to accurate model the large are fields generated at the irradiation/measurement stage of HollandPTC operating in it’s passively scattered field configuration.

4. Discussion and Conclusion

A Geant4 simulation platform of the HollandPTC R&D beamline was developed, trained through comparison with three energy experimental datasets, and then benchmarking against three independent experimental datasets. The agreement between experimental and Geant4 simulation platform results in the training phase was assessed by comparing the FWHM, FWTM, initial mean energy and energy spread. With the optimisation beam parameters the Geant4 simulation platform was able to reproduce both experimental the beam envelope evolution and dose-depth profile data outlined in Section 3.1 to a high level of accuracy of the HollandPTC R&D beamline operating in its pencil beam configuration. These optimised non-symmetrical Gaussian pencil beam parameters then served as the basis for energy dependent surrogate functions (see Section

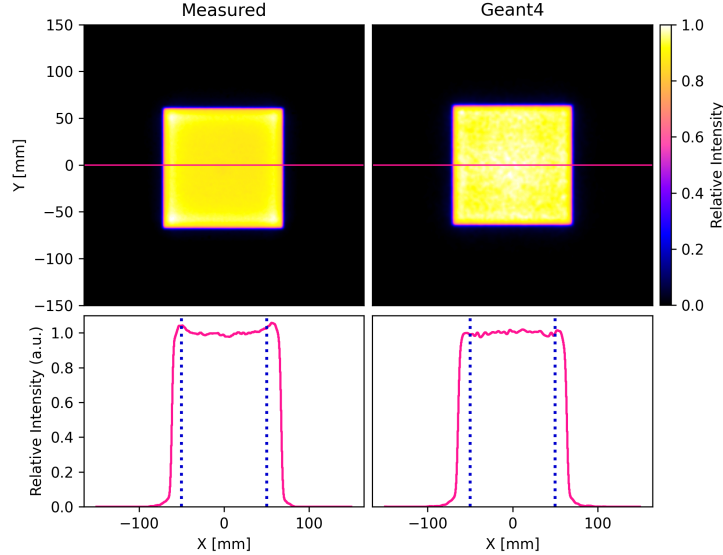


Figure 9: Experimental and Geant4 100 mm \times 100 mm fields (top) and their respective central x -axis lines profiles (bottom) generated at the irradiation/measurement stage of the HollandPTC R&D beamline operating in it's passively scattered field configuration. Here the pink horizontal lines (top) represent where the central x -axis lines profiles were taken, and the blue dotted lines outline the target field 100 mm \times 100 mm of interest.

2.2) which were used in the Geant4 simulation platforms experimental benchmarking against three independent experimental datasets. It was shown that for each of the three different experimental benchmarking trials that the Geant4 simulation platform was able to accurate model the HollandPTC R&D beamline operating in both its pencil beam and passively scattered field configuration over its energy range of operation (70 to 240 MeV)

The splitting of the Geant4 simulation platform development into a training and experimental benchmarking phase was crucial in verifying the physical accuracy and reliability for it's application to planning future experimental radiobiological studies at the HollandPTC R&D beamline. However, there was one key design choice in the development of the Geant4 simulation platform which differed to the majority of previous similar studies that ensured this would be possible: the implementation of an experimental trained six degree of freedom non-symmetrical Gaussian pencil beam surrogate model that only requires the HollandPTC's cyclotron mean extraction proton energy as input [21, 22, 23, 24, 25]. Evidence of both the physical accuracy and reliability of this approach was illustrated in the experimental benchmarking phase with it shown that the developed Geant4 simulation platform was able to model the emerging proton beam structure, energy, and energy spread at the Kapton vacuum pipe

exit window, and then it's propagation along the HollandPTC R&D beamline in both it's pencil beam and passively scattered field configuration. This would not of been possible without the combined energy dependent 2D Gaussian function fitting and Sum of Squared Errors (SSE) metric σ_x , σ_y , θ_x and θ_y parameter optimisation approach outlined in Section 2.2. Given the success of this key design choice, it is hoped that this approach will be adopted as a standard for future studies that develop Geant4 simulation platforms of experimental proton irradiation beamlines intended for fundamental radiobiological studies.

This work both developed and characterised the performance of a Geant4 simulation platform for the HollandPTC R&D beamline to enable the in-silico planning and optimisation of future radiobiological studies at the HollandPTC. It is the first step in an on-going joint Delft University of Technology (Netherlands), Erasmus Medical Centre (Netherlands), HollandPTC (Netherlands) and Swinburne University of Technology (Australia) research program that aims to develop novel instrumentation and leverage nanoscale simulation of proton induced DNA damage to undertake high quality physics-biological linked radiobiological proton irradiation studies. Further work is already underway to expand this Geant4 simulation platform to include the novel radiobiological endstations underdevelopment at HollandPTC outlined in Rovituso et al. [18], and explore the relationship between proton Linear Energy Transfer (LET) and biological outcome in the FaDu HNSCC cell line.

Acknowledgements

This work was partially funded by Varian Medical Systems (a Siemens Healthineers Company), and the simulations undertaken on the Dutch national e-infrastructure with the support of SURF Cooperative (Grant No: EINF-486 (2020)). J. M. C. Brown was supported by a Veni fellowship from the Dutch Organization for Scientific Research (NWO Domain AES Veni 16808 (2018)) during the time of this study.

References

- [1] Langendijk J. A., Doornaert P., Verdonck-de Leeuw I. M., Leemans C. R., Aaronsen N. K. and Slotman B. J. (2008). *Impact of late treatment-related toxicity on quality of life among patients with head and neck cancer treated with radiotherapy*, Journal of Clinical Oncology 26(22): 3770-3776.
- [2] Palm Å. and Johansson K. A. (2007). *A review of the impact of photon and proton external beam radiotherapy treatment modalities on the dose distribution in field and out-of-field; implications for the long-term morbidity of cancer survivors*, Acta Oncologica 46(4): 462-473.
- [3] Cozzi L., Fogliata A., Lomax A. and Borsi A. (2001). *A treatment planning comparison of 3D conformal therapy, intensity modulated photon therapy and proton therapy for treatment of advanced head and neck tumours*, Radiotherapy and Oncology 61(3): 287-297.

- [4] Langendijk J. A., Lambin P., De Ruysscher D., Widder J., Bos M. and Verheij M. (2013). *Selection of patients for radiotherapy with protons aiming at reduction of side effects: the model-based approach*, Radiotherapy and Oncology 107(3): 267-273.
- [5] Widder J., Van Der Schaaf A., Lambin P., Marijnen C. A., Pignol J. P., Rasch C. R., Slotman B. J., Verheij M. and Langendijk J. A. (2016). *The quest for evidence for proton therapy: model-based approach and precision medicine*, International Journal of Radiation Oncology* Biology* Physics 95(1): 30-36.
- [6] Nguyen M. L., Cantrell J. N., Ahmad S. and Henson C. (2021). *Intensity-modulated proton therapy (IMPT) versus intensity-modulated radiation therapy (IMRT) for the treatment of head and neck cancer: A dosimetric comparison*, Medical Dosimetry 46(3): 259-263.
- [7] Borsi A., Placidi L., Pica A., Ahlhelm F. J., Walser M., Lomax A. J. and Weber D. C. (2020). *Pencil beam scanning proton therapy for the treatment of craniopharyngioma complicated with radiation-induced cerebral vasculopathies: A dosimetric and linear energy transfer (LET) evaluation*, Radiotherapy and Oncology 149: 197-204.
- [8] Lin S. H., Hobbs B. P., Verma V., Tidwell R. S., Smith G. L., Lei X., Corsini E. M., Mok I., Wei X., Yao L. and Wang X. (2020). *Randomized phase IIB trial of proton beam therapy versus intensity-modulated radiation therapy for locally advanced esophageal cancer*. Journal of Clinical Oncology 38(14): 1569.
- [9] Price J., Hall E., West C. and Thomson D. (2020). *TORPEdO—a phase III trial of intensity-modulated proton beam therapy versus intensity-modulated radiotherapy for multi-toxicity reduction in oropharyngeal cancer*, Clinical Oncology 32(2): 84-88.
- [10] Kim T. H., Koh Y. H., Kim B. H., Kim M. J., Lee J. H., Park B. and Park J. W. (2021). *Proton beam radiotherapy vs. radiofrequency ablation for recurrent hepatocellular carcinoma: A randomized phase III trial*, Journal of Hepatology 74(3): 603-612.
- [11] Bertolet A., Abolafath R., Carlson D. J., Lustig R. A., Hill-Kayser C., Alonso-Basanta M. and Carabe A. (2022). *Correlation of LET with MRI changes in brain and potential implications for normal tissue complication probability for patients with meningioma treated with pencil beam scanning proton therapy*, International Journal of Radiation Oncology* Biology* Physics 112(1): 237-246.
- [12] Kim K., Yu J. I., Park H. C., Yoo G. S., Lim D. H., Noh J. M. and Jeong W. K. (2022). *A phase II trial of hypofractionated high-dose proton beam therapy for unresectable liver metastases*, Radiotherapy and Oncology 176: 9-16.

- [13] Mascia A. E., Daugherty E. C., Zhang Y., Lee E., Xiao Z., Sertorio M., Woo J., Backus L. R., McDonald J. M., McCann C. and Russell K. (2023). *Proton FLASH radiotherapy for the treatment of symptomatic bone metastases: the FAST-01 nonrandomized trial*, *JAMA Oncology* 9(1): 62-69.
- [14] Holland Proton Therapy Centre [Netherlands] (2018), *First successful treatment with proton therapy in HollandPTC*, <https://www.hollandptc.nl/1e-patient-succesvol-bestraald-hollandptc-open-voor-patientenzorg-en-onderzoek/>.
- [15] Agostinelli S. et al. (2003). *Geant4-a simulation toolkit*, Nuclear Instruments and Methods in Physics Research Section A 506(3): 250-303.
- [16] Allison J. et al. (2006). *Geant4 developments and applications*, IEEE Transactions on Nuclear Science 53(1): 270-278.
- [17] Allison J. et al. (2016). *Recent developments in Geant4*, Nuclear Instruments and Methods in Physics Research Section A 835: 186-225.
- [18] Rovituso M., Groenendijk C. F., van der Wal E. , van Burik W, Ibrahim A., Rituerto Prieto H., Brown J. M. C., Weber U., Simeonov Y., Fontana M., Lathouwers D., van Vulpen M. and Hoogeman M. (2023). *Characterisation of the HollandPTC R&D proton beamline for physics and radiobiology studies*, In Prep. for *Physica Medica*.
- [19] Arce P. et al. (2021). *Report on G4-Med: a Geant4 benchmarking system for medical physics applications developed by the Geant4 Medical Simulation Benchmarking Group*, *Medical Physics* 48(1): 19-56.
- [20] Bortfeld T. (1997). *An analytical approximation of the Bragg curve for therapeutic proton beams*, *Medical Physics* 24(12): 2024-2033.
- [21] Paganetti H., Jiang H., Lee S. Y. and Kooy H. M. (2004). *Accurate Monte Carlo simulations for nozzle design, commissioning and quality assurance for a proton radiation therapy facility*, *Medical Physics* 31(7): 2107-2118.
- [22] Dowdell S. J., Clasie B., Depauw N., Metcalfe P., Rosenfeld A. B., Kooy H. M., Flanz J. B. and Paganetti H. (2012). *Monte Carlo study of the potential reduction in out-of-field dose using a patient-specific aperture in pencil beam scanning proton therapy*, *Physics in Medicine & Biology* 57(10): 2829.
- [23] Fracchiolla F., Lorentini S., Widesott L. and Schwarz M. (2015). *Characterization and validation of a Monte Carlo code for independent dose calculation in proton therapy treatments with pencil beam scanning*, *Physics in Medicine & Biology* 60(21): 8601.
- [24] Liu H., Li Z., Slopsema R., Hong L., Pei X. and Xu X. G. (2019). *TOPAS Monte Carlo simulation for double scattering proton therapy and dosimetric evaluation*, *Physica Medica* 62: 53-62.

[25] Tommasino F., Rovituso M., Bortoli E., La Tessa C., Petringa G., Lorentini S., Verroi E., Simeonov Y., Weber U., Cirrone P. and Schwarz M. (2019). *A new facility for proton radiobiology at the Trento proton therapy centre: Design and implementation*, *Physica Medica* 58: 99-106.